Appl. Phys. B 60, 145–153 (1995)

Applied Physics B Lasers and Optics

Localization of atoms in light fields: Optical molasses, adiabatic compression and squeezing

S. Marksteiner[1,2], R. Walser[1,2], P. Marte[1,2], P. Zoller[1,2]

[1]Joint Institute for Laboratory Astrophysics, University of Colorado, Boulder, CO 80309-0440, USA
[2]Institut für Theoretische Physik, Universität Innsbruck, A-6020 Innsbruck, Austria
(Fax: +43-512/218-5173, E-mail: Stefan.Marksteiner@uibk.ac.at, Reinhold.Walser@uibk.ac.at, Peter.Marte@uibk.ac.at, Peter.Zoller@uibk.ac.at)

Received: 10 August 1994 / Accepted: 17 October 1994

Abstract. We present a theoretical study of the localization of atoms with an angular momentum J_g=3 to J_e=4 transition (e.g., chromium atoms) in quantized optical molasses created by two counterpropagating linearly polarized laser beams. We study the localization as a function of the potential depth, the angle between the polarizations and the interaction time with the molasses in the low-intensity limit, and discuss the possibility of adiabatic compression and squeezing of the atomic distribution.

PACS: 32.80.Pj; 42.50.Vk; 81.15.−z

Optical potentials due to laser light allow the focusing of atoms to sub-wavelength structures during deposition on a substrate. Interest in these techniques derives from the possibility that an inherently parallel approach can be developed for fabricating nanometer-size structures. In recent atomic beam experiments, Timp et al. [1] and McClelland et al. [2] have demonstrated the writing of narrow lines of sodium and chromium atoms by focusing with atom lenses formed by a standing-wave laser light. We note that these experiments are performed in the limit of coherent atom optics [1, 3–7], i.e., in the limit where there are no spontaneous emissions during the interaction with the laser light.

Localization of atoms to a fraction of the laser wavelength can also be obtained by transverse polarization-gradient cooling of an atomic beam. In such an optical molasses configuration, two counterpropagating laser beams lead to a damping of the atomic motion and give rise to an optical potential [8–10]. The periodic optical potential supports a band structure corresponding to a quantization of the atomic vibrations in the potential wells. Laser cooling leads to the accumulation of the atoms in the few lowest vibrational energy states and localization of the atoms in the potential minima [11–13]. The purpose of the present paper is to present, within a fully quantum mechanical framework, results of a quantitative study of the localization of atoms in optical molasses and to investigate the possibility of further subsequent narrowing of the atomic distribution by adiabatic compression or by "squeezing".

Dedicated to H. Walther on the occasion of his 60th birthday

In optical molasses, the vibrational eigenstates become more localized when the depth of the optical potential U_0 is increased. On the other hand, in steady-state laser cooling, the populations of the few lowest states exhibit a maximum (lowest temperature) at a certain value $U_{0\max}$ [8, 9, 11]. We will show in this paper that these two effects cancel each other so that the steady-state localization is essentially constant for $U_0 > U_{0\max}$. In our calculations, we will assume a low intensity-limit where the potential $U(z)$ is proportional to the local intensity $I(z)$ of the cooling lasers which, for steady-state molasses, gives rise to the lowest temperatures. To be specific, we will concentrate on an angular momentum $3 \rightarrow 4$ transition as realized, for example, in chromium atoms [2].

The localization obtained in optical molasses can be improved by a subsequent adiabatic compression [14] and/or "squeezing" of the atomic distribution. In a harmonic oscillator approximation for the optical potential induced by a standing-wave laser field, $U(z) = U_0 \sin(k_L z)^2 \approx U_0(k_L z)^2 \equiv m\omega^2 z^2/2$ the size of the ground state is given by $\Delta a_0 = (\hbar/2m\omega)^{1/2}$ with ω the oscillation frequency of the atom in the optical potential, m the mass of the atom and k_L the wave vector of the laserfield. For adiabatic compression, the potential depth is increased to better localize the vibrational eigenstates. If the time scale of the variation of the potential is small compared to the oscillation period in the wells, but fast on the scale given by optical pumping, the population of these levels obtained from laser cooling will remain constant during the adiabtic process, resulting in an overall compression of the atomic distribution. Since below saturation, the optical potential is proportional to the light intensity, the compression achieved in this way is $\Delta z_f/\Delta z_i = (\omega_i/\omega_f)^{1/2} \equiv (I_i/I_f)^{1/4}$, with $\Delta z_{i(f)}$ the inital (final) width of the distribution and $\omega_{i(f)}$ the initial (final) oscillation frequency which is proportional to the square root of the laser intensity $I_{i(f)}$. While the improvement of the localization goes only with the fourth root of the ratio of the initial to final intensity, adiabatic compression has the advantage of being independent of the longitudinal velocity of the atom in an atomic beam (interaction time) over a wide parameter range.

A second possibility to improve localization is by generation of a squeezed state of motion in the (approximately) harmonic part of the optical potential. It is well known that a non-adiabatic frequency variation leads to the formation of a wave packet, which, for certain times, will be squeezed in position space, $\Delta z \ll a_0$ with a_0 the oscillator ground state [15–17]. A modulation of the optical potential between $\omega_i \leq \omega \leq \omega_f$ leads to an improved localization $\Delta z_f/\Delta z_i = (\omega_i/\omega_f) \equiv (I_i/I_f)^{1/2}$. These squeezing cycles can be repeated, resulting in a more and more squeezed atomic distribution. In a harmonic-oscillator potential there is – at least in principle – no lower bound for the attainable squeezing [15, 17]. We emphasize, however, that a squeezed wave packet corresponds to a superposition of an increasing number of harmonic-oscillator energy eigenstates. Thus, the optimum squeezing that can be obtained in an optical potential with period a is limited by $\Delta z_{\max} \propto a_0^2/a \ll a_0$ [18].

The paper is organized as follows. In Sect. 1, we give a brief summary of the basic equations for laser cooling in one–dimensional optical molasses. Section 2 presents our results for the localization of atoms for a standing-wave laser configuration with two counterpropagating linearly polarized light waves. Finally, in Sect. 3, we discuss the basic mechanisms of time-dependent compression techniques and compare results obtained within the harmonic-oscillator approximation to simulations of adiabatic compression of a precooled molasses.

1 Basic equations

In this section we summarize and review the basic equations of one-dimensional (1D) transverse laser cooling to identify the physical parameters in our model and establish our notation. For details, refer to [8–10]. In our 1D, model we consider a two-level atom with a Zeeman substructure corresponding to an angular momentum J_g to J_e transition in a laser configuration consisting of two counterpropagating light beams with linear polarization. For the specific calculations below, we assume $J_g = 3 \rightarrow J_e = 4$ corresponding to Cr. The angle between the polarizaton vectors is denoted by θ.

We are interested in laser intensities well below saturation $s \ll 1$ which give rise to the lowest temperatures corresponding to the largest ground-state population. The saturation parameter is defined as $s = \frac{1}{2}\Omega^2/(\Delta^2 + \frac{1}{4}\Gamma^2)$, with $\Omega = 2\mathscr{E}d/\hbar$ the Rabi frequency, d the dipole-matrix element on the outermost Zeeman transition $M_g = J_g \rightarrow M_e = J_e$, Γ the spontaneous decay rate, and $\Delta = \omega_L - \omega_{eg}$ the laser detuning. Elimination of the excited-state manifold leads to Generalized Optical Bloch Equations (GOBE) for the ground-state density matrix $\rho_{gg}(t)$ [19] ($\hbar = 1$)

$$\dot{\rho}_{gg} = -\mathrm{i}\left(h_{\mathrm{eff}}\rho_{gg} - \rho_{gg}h_{\mathrm{eff}}^{\dagger}\right) + 2\gamma_0 \sum_{\sigma=0,\pm1} \int_{-k}^{+k} \mathrm{d}u N_\sigma(u)[B_\sigma(\hat{z})\mathrm{e}^{-\mathrm{i}u\hat{z}}]\,\rho_{gg}[\mathrm{e}^{\mathrm{i}u\hat{z}}B_\sigma^{\dagger}(\hat{z})]\,, \quad (1)$$

with a non-Hermitian effective Hamiltonian

$$h_{\mathrm{eff}} = \frac{\hat{p}^2}{2M} + \frac{s}{2}\left(\Delta - \mathrm{i}\frac{\Gamma}{2}\right)\mathscr{D}(\hat{z})\mathscr{D}^{\dagger}(\hat{z})\,. \quad (2)$$

The first two terms on the right-hand side of (1) correspond to a time evolution due to the Hamiltonian h_{eff}, while the last term describes the return of the atomic electron to the ground state by optical pumping.

The Hermitian part of h_{eff} describes the coherent 1D motion of a particle in the periodic optical potential

$$U(z) = -\frac{1}{2}s\Delta\mathscr{D}(\hat{z})\mathscr{D}^{\dagger}(\hat{z}), \quad (3)$$

as given by the ac-Stark shift of the various Zeeman sublevels, where $\mathscr{D}(\hat{z})$ denotes the dipole operator connecting the ground and excited states. In the following, we will refer to $U_0 = -s\Delta/2$ as the potential depth. Since our laser configuration involves no π-polarized light component, this coherent evolution couples only states that are connected by a σ_+–σ_- Raman transition, i.e., only states of even and odd M_g are coupled by $U(z)$. The anti-Hermitian part in (2) describes a damping due to optical pumping with $\gamma_0 = s\Gamma/4$, the optical pumping rate between the ground-state levels. The operators $B_\sigma(\hat{z}) = A_\sigma\mathscr{D}^{\dagger}(\hat{z})$ in the last term of (1) describe a Raman transition, corresponding to absorption of a laser photon ($\mathscr{D}^{\dagger}$) followed by spontaneous emission of a photon (the operator A_σ) with light polarization $\sigma = 0, \pm1$ and angular distribution $N_{0,\pm1}u$. Here, $N_0(u) = 3/4[1 - (u/k)^2]$ and $N_{\pm1}(u) = 3/8[1 + (u/k)^2]$ [19] are the angular distributions of the emitted photons for polarization σ. The Liouville operator in the GOBE (1) is invariant under $\lambda/2$ translations, and there exists an (infinitely extended) periodic steady-state density matrix with this symmetry. All the results reported below correspond to this periodic distribution.

2 Localization in 1D optical molasses

In this section, we will concentrate on a $J_g = 3$ to $J_e = 4$ transition. This corresponds, for example, to chromium atoms [2] driven on the $7S_3$–$7P_4$ transition. We note that this transition is not a pure two–level system since there is a "leak" of the excited state to the $5D$ levels with a branching ratio of about 1:500. We ignore this leakage rate, since, typically, the steady state of the optical molasses is obtained in a time much shorter than this decay rate. We note that populations of the vibrational levels for a $F_g = 3$ to $F_e = 4$ transition were already discussed in our previous work on the spectrum of resonance fluorescence of ^{87}Rb [9].

The laser configuration consists of two counterpropagating light beams with linear polarizations. We denote the angle between the polarizaton vectors by θ. In this configuration the electric field can be written as

$$\mathbf{E}_{\mathrm{cl}}^{+}(z,t) = \mathscr{E}\sqrt{2}[\cos(kz)\mathbf{e}_+ - \cos(kz+\theta)\mathbf{e}_-]\mathrm{e}^{-\mathrm{i}\omega_L t}. \quad (4)$$

Here $\mathscr{E}$ is the light amplitude, ω_L denotes the laser frequency, z is the coordinate along the light propagation axis (which is also the quantization axis for the atom), and $\mathbf{e}_\pm = \mp\frac{1}{\sqrt{2}}(\hat{\mathbf{x}} \pm \mathrm{i}\hat{\mathbf{y}})$ are spherical unit vectors.

2.1 Optical potentials

In this subsection, we will discuss those characteristics of the ac-Stark-shift potential that are important for the localization

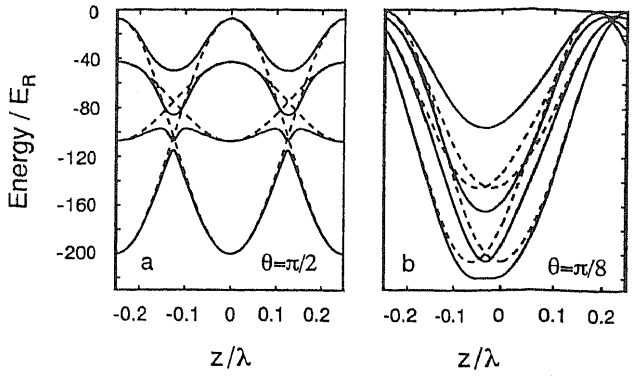

Fig. 1a,b. Diabatic (*dashed*) and adiabatic (*solid*) potentials for the odd M_g Zeeman sublevels in a J_g=3→J_e=4 transition as a function of position for U_0=100 E_R, (**a**) $\theta=\pi/2$, (**b**) $\theta = \pi/8$

of atoms. The potential (3) is a local operator that operates in the space spanned by the internal degrees of freedom at every point in space, and, therefore, its representation in the basis of the Zeeman sublevels is a position-dependent matrix. The laser configurations considered here involve only $\sigma_\pm$ components and, therefore, all of the even ground-state Zeeman sublevels are coupled by coherent Raman processes. The same is true for the odd sublevels. The coupling between the odd and even ground states is only due to spontaneous emission and, therefore, the potential matrix can be factorized into two submatrices corresponding to the odd and even submanifold. We will denote the parts of the optical potential that correspond to odd and even sublevels by U_1 and U_2, respectively. Figure 1 shows the adiabatic (diabatic) potentials corresponding to the eigenvalues (diagonal elements) of the potential matrix U_1 of the odd Zeeman ground states for two different angles between the polarizations of the laser beams.

Let us first turn to Fig. 1a, for which $\theta = \pi/2$. This corresponds to the familiar lin⊥lin configuration, as first discussed for a $1/2 \rightarrow 3/2$ transition by Castin and Dalibard [8]. In this case the nodes of one standing-wave spatially coincide with the antinodes of the other [4]. We find that the diabatic potentials of the outermost two sublevels $M_g = \pm 3$ are sinusoidal and have their minima at positions with pure σ_+ and σ_- light, respectively. This leads to a lowest adiabatic potential that has a periodicity of $\lambda/4$ (for a detailed study of this symmetry, see [20]). The other states give rise to adiabatic potentials that lie above the threshold of the lowest one. In Fig. 1b, we show the same plot but for an angle $\theta = \pi/8$ between the polarizations. In this case, the two standing σ_+ and σ_- light waves are shifted with respect to each other and, therefore, their nodes move closer together. This leads to a corresponding shift of the diabatic potentials and a $\lambda/2$ symmetry for the adiabatic potentials. In addition, the potentials are somewhat deeper, so that we expect their Bloch wave functions to be better localized than the ones in the lin⊥lin configuration. Another difference from Fig. 1a is that the other states give rise to adiabatic potentials that are no longer above the threshold of the lowest one.

In the following, we will quantitatively investigate the localization of atoms in the molasses created by the two laser configurations mentioned above as a function of the most important experimental parameters, i.e., the potential

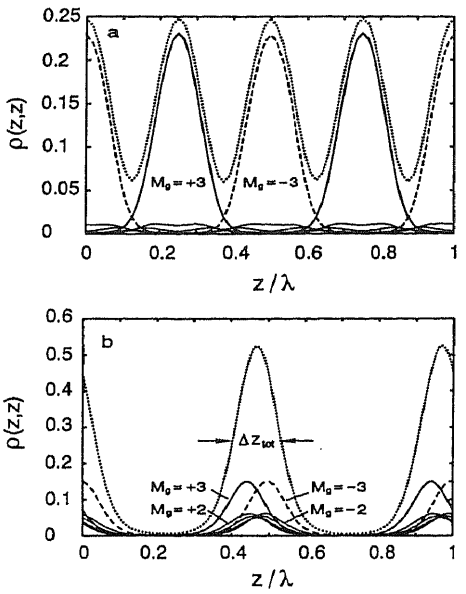

Fig. 2a,b. Spatial distribution of the various Zeeman sublevels (*solid line* M_g = +3, *dashed line* M_g = −3, *thin solid lines* M_g = −2, . . . , +2) and corresponding total distribution (*dotted line*) for U_0=100 E_R, γ_0 = 10 ω_R , (**a**) $\theta=\pi/2$ and (**b**) $\theta = \pi/8$. The *arrows* indicate the FWHM of the total distribution

depth U_0 and the interaction time with the molasses. To calculate this spatial localization, we solve the GOBE (1) using a Monte-Carlo wave-function technique [9, 19].

2.2 *The lin⊥lin configuration ($\theta = \pi/2$)*

Figure 2a shows the spatial distribution of the various Zeeman sublevels (i.e., the diagonal part of the density matrix $\langle z, M_g | \rho_{gg} | z, M_g' \rangle$) for a potential depth of U_0 = 100 E_R as a function of position. Here, $E_R = \hbar\omega_R = \hbar^2 k_L^2/2m$ denotes the recoil energy. The dotted line represents the total spatial distribution of the atoms (summed over all Zeeman sublevels). We find 87% of the population in the two outermost Zeeman sublevels $M_g = \pm 3$, i.e. in the lowest adiabatic potential. The distribution of the $M_g = \pm 3$ sublevel shows a $\lambda/2$ periodicity, whereas the *total* distribution exhibits a $\lambda/4$ period.

We performed a series of simulations for various potential depths ranging from 60 to 1000 E_R and found that, at large enough U_0 the distribution in Fig. 2a is rather insensitive to the potential depth. Although the width of the various peaks decreases rapidly with increasing U_0 in the range of 60 to 100 E_R, it more or less approaches a constant value for U_0 larger than 200 E_R (for a quantitative discussion of this see Sect. 2.3). We, therefore, conclude that although the lin⊥lin molasses leads to a good localization of the *individual* Zeeman sublevels (line separation : FWHM ≈ 4 : 1), the lines of the *total* distribution overlap in such a way that the total distribution is essentially sinusoidal, with a background that is on the order of 25% of the peak hight (Fig. 2a). This is due to the $\lambda/4$ dislocation of the minima of the diabatic potentials of the sublevels $M_g = \pm 3$.

2.3 The lin–∠–lin configuration ($\theta = \pi/8$)

According to (4), the angle θ between the polarization vectors is related to the phase shift between the σ^+ and σ^- standing waves of the electric field. For $\theta \neq \pi/2$, the two minima of the adiabatic potentials move together: this is illustrated in Fig. 1b for $\theta = \pi/8$, where the distance between adjacent $M_g = -3$ and $M_g = +3$ minima is approximately $\lambda/16$. Since laser cooling leads to a localization in these potential minima, we expect that the $M_g = \pm 3$ distributions are now strongly overlapping and that this configuration leads to lines with periodicity $\lambda/2$. Since the temperature in optical molasses tends to increase for decreasing $\theta < \pi/2$ [20], and the vibrational ground state in the potential Fig. 1b is wider than that in Fig. 1a, we expect less localization on an *absolute* scale but a better *relative* localization (width of the lines divided by their distance).

The spatial distribution of the various Zeeman sublevels for the same parameters as in Fig. 2a is shown in Fig. 2b. We find that the population in the two outermost sublevels $M_g = \pm 3$ has dropped to about 50%, and that each of the inner sublevels carries approximately 10% of the population. We find good total localization, even in the case of moderate potential depth ($U_0 = 100\ E_R$ in Fig. 2a). The width of the various sublevels is even slightly smaller than in the $\theta=\pi/2$ case. This is due to the better localization of the Bloch levels in the deeper adiabatic potentials (Fig. 1b).

To investigate the dependence of the localization on the potential depth, we define the linewidth Δz (either one individual sublevel or the total distribution) to be the FWHM of a Gaussian which we fit to the given spatial distribution (Fig. 2b). The results for a series of steady-state simulations with various potential depths are presented in Fig. 3. We find that for small potential depths, up to approximately 100 E_R, Δz_{tot} decreases strongly with increasing U_0. This is due to the fact that the temperature of the molasses and, therefore, the population of the various bands is more or less constant (the optimum cooling potential is 80 E_R[9]), whereas the Bloch states themselves are better localized the deeper the potential is. A further increase of the potential depth beyond 100 E_R still decreases the width of the lowest vibrational states but the temperature and, therefore, the population of higher levels increases, since we are no longer in the regime of optimal laser cooling. These two competing effects lead to the saturation of the localization that takes place for $U_0 > 200\ E_R$.

2.4 Time scale of localization

In an atomic-beam experiment with transverse cooling, the longitudinal velocity of the atoms leads to a certain interaction time for the transverse localization. In [2], an approximately 2 cm long optical molasses was utilized to transversely cool a thermal chromium beam of temperature 1500°C. (Note that the actual deposition in this experiment is not due to the localization in the molasses, but rather to the coherent focusing of the atoms in a far off-resonant laser standing wave, which we will discuss in Sect. 3.) This leads to an interaction time of approximately 20 μs, which corresponds to about 100 spontaneous emission lifetimes.

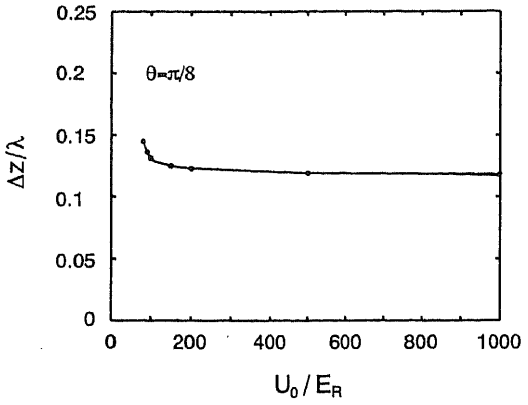

Fig. 3. FWHM of the total distribution versus potential depth, calculated with $\gamma_0 = 10\ \omega_R$ and $\theta = \pi/8$. The *dots* show the individual simulation points

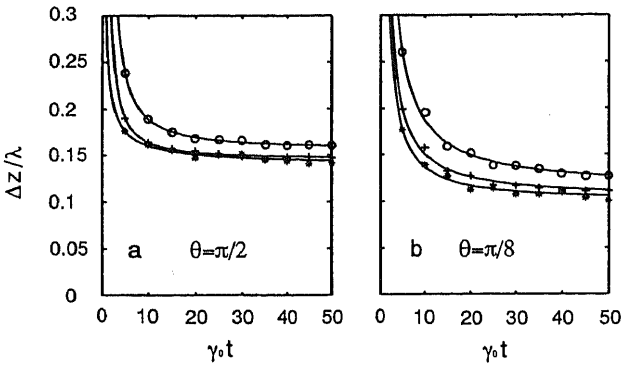

Fig. 4. a FWHM of the $M_g = \pm 3$ sublevels vs interaction time (in units of the optical pumping time $1/\gamma_0$) for (*top* to *bottom*) U_0=100, 200, 500 E_R and $\theta = \pi/2$, $\gamma_0 = 10\ \omega_R$. **b** Same as **a**, but for $\theta = \pi/8$

Therefore, the question arises: can the steady state, which was assumed for the calculations in Sects. 2.2 and 2.3, be reached within this interaction time?

To answer this question, we performed transient simulations of the GOBE (1), by starting with an initial distribution that is an incoherent superposition of plane waves. The momentum distribution was assumed to be a (Doppler precooled) Gaussian with a half-width of 12 $\hbar k_L$, and the internal distribution was assumed to be distributed equally and incoherently among the various Zeeman sublevels. In these simulations, we further neglected any variation of the intensity of the laser beams with position. The results are shown in Figs. 4a,b as a function of optical pumping times $1/\gamma_0$ [21].

Figure 4a shows the width $\Delta z_{\pm 3}$ of the outermost Zeeman sublevels as a function of time for the lin⊥lin configuration and for various potential depths. A $\Delta z_{\pm 3}/\lambda$ equal to 0.27, corresponds to a spatial distribution with peak-to-valley ratio of 0.1, whereas $\Delta z_{\pm 3}/\lambda = 0.19$ and 0.16 correspond to peak-to-valley ratios of 0.01 and 0.001, respectively. The localization takes place on a rather short time scale, approximately $15/\gamma_0$, more or less independent of the potential depth. Figure 4b shows the same characteristics for the $\pi/8$ configuration. The localization time is increased by a factor of 2, which is due to the less-efficient cooling in this laser

configuration. Furthermore, the steady state $\Delta z_{\pm 3}$ is smaller than that of the lin⊥lin configuration.

3 Compression of the transverse spatial distribution

The preceding sections described a full quantum mechanical treatment of the 1D transverse-cooling process of an atomic beam. We have shown that strong localization occurs within the potential wells corresponding to the individual magnetic sublevels. Now, we address the question of whether further narrowing of the position width can be achieved, once optimal cooling has been obtained. We first discuss the possibility of adiabatic compression and squeezing of the spatial distribution obtained in optical molasses within a harmonic-oscillator approximation [15–17]. Then, we compare these analytical predictions with a full calculation of adiabatic compression of optical molasses on a $3 \rightarrow 4$ transition.

3.1 Spatial compression in the harmonic approximation

Expanding the periodic potential in the vicinity of a minimum $U(z,t) = U_0(t)\sin(k_L z)^2 \approx U_0(t)(k_L z)^2$ yields a harmonic Hamilton operator

$$\hat{H}(t) = \frac{\hat{p}^2}{2m} + \frac{1}{2}m\omega(t)^2\hat{z}^2, \tag{5}$$

with $\omega(t) = [(2k_L^2/m)U_0(t)]^{1/2}$ and a maximal permissible aperture $a = \lambda_L/2$, which is equal to the periodicity of the potential. Assuming a thermal quantum state in a harmonic oscillator, we have

$$\begin{aligned}\hat{\rho}_{th} &= e^{-\hat{H}(t_i)/k_B T}\frac{1}{\mathrm{Tr}(e^{-\hat{H}(t_i)/k_B T})} \\ &= 2\sinh(\beta/2)\sum_n |n\rangle\langle n| e^{-\beta(n+1/2)},\end{aligned} \tag{6}$$

where $\beta = \hbar\omega(t_i)/(k_B T)$ and $|n\rangle$ are the energy eigenstates. The position and momentum width at the initial instant t_i, which can be obtained from averages over the thermal state $\langle\ldots\rangle = \mathrm{Tr}(\hat{\rho}_{th}\ldots)$, are

$$\Delta^2\hat{z}(t_i) = \langle\hat{z}(t_i)^2\rangle - \langle\hat{z}(t_i)\rangle^2 = a_0^2\frac{1}{\tanh(\beta/2)}, \tag{7}$$

$$\Delta^2\hat{p}(t_i) = \langle\hat{p}(t_i)^2\rangle - \langle\hat{p}(t_i)\rangle^2 = \frac{\hbar^2}{4a_0^2}\frac{1}{\tanh(\beta/2)}, \tag{8}$$

where $a_0 = (\hbar/2m\omega_i)^{1/2}$ is the width of the initial ground state ($\omega(t_i) = \omega_i$). It is a consequence of the parity and the rotational symmetry of $\hat{\rho}_{th}$, seen, for example, from a Wigner representation in phase space, that the expectation values $\langle\hat{z}(t_i)\rangle$, $\langle\hat{p}(t_i)\rangle$ and $\Delta^2[\hat{z}(t_i)\hat{p}(t_i) + \hat{p}(t_i)\hat{z}(t_i)]$ vanish.

The solutions of Heisenberg's equation for position and momentum operators $\hat{z}(t)$, $\hat{p}(t)$ are obtained immediately since they are linear. By defining a transfer matrix $\underline{S}(t)$ from the fundamental solutions of the classical equation of motion

$$\frac{d^2}{dt^2}f_{i=1,2}(t) = -\omega(t)^2 f_i(t), \tag{9}$$

which is of the same functional form, we find

$$\begin{pmatrix}\hat{z}(t)\\ \hat{p}(t)\end{pmatrix} = \underline{S}(t)\begin{pmatrix}\hat{z}(0)\\ \hat{p}(0)\end{pmatrix} \text{ with}$$

$$\underline{S}(t) = \begin{pmatrix}f_1(t) & f_2(t)/m\\ mf_1(t)' & f_2(t)'\end{pmatrix}, \tag{10}$$

and $\underline{S}(t_i) = \mathbf{1}$. Since $\underline{S}(t)$ is symplectic, $\mathrm{Det}[\underline{S}(t)] = 1$ which implies that the commutation relations are preserved. Thus, position and momentum width are given by

$$\begin{aligned}\Delta^2\hat{z}(t) &= \Delta^2\hat{z}(t_i)f_1(t)^2 + \frac{\Delta^2\hat{p}(t_i)}{m^2}f_2(t)^2 \\ &= \Delta^2\hat{z}(t_i)\left[f_1(t)^2 + \omega_i^2 f_2(t)^2\right],\end{aligned} \tag{11}$$

$$\begin{aligned}\Delta^2\hat{p}(t) &= m^2\Delta^2\hat{z}(t_i)f_1(t)'^2 + \Delta^2\hat{p}(t_i)f_2(t)'^2 \\ &= \Delta^2\hat{p}(t_i)\left[\frac{1}{\omega_i^2}f_1(t)'^2 + f_2(t)'^2\right].\end{aligned} \tag{12}$$

Depending on the rate of frequency change there are several discernable limits.

3.1.1 Adiabatic compression. The adiabatic limit is appropriate if the frequency changes significantly only after a large number of oscillation periods have passed, i.e.,

$$\left|\frac{\omega(t)'}{\omega(t)^2} = 2\tan\varphi(t)\right| \ll 1. \tag{13}$$

Together with a WKB ansatz $f(t) = \exp[i\Phi(t)]$, this condition leads to the adiabatic approximation for the transfer matrix $\underline{S}_{adiab}(t)$ (see the Appendix for details). From these solutions we can infer that the position variance diminishes according to

$$\begin{aligned}\Delta^2\hat{z}(t) &= \Delta^2\hat{z}(t_i)\frac{\omega_i}{\omega(t)} \\ &\times\left\{1 + \tan[\varphi(t_i)]\sin[2\int_{t_i}^{t}\omega(t_1)dt_1] + \mathcal{O}[\varphi(t)^2]\right\},\end{aligned} \tag{14}$$

while the momentum width increases as

$$\begin{aligned}\Delta^2\hat{p}(t) &= \Delta^2\hat{p}(t_i)\frac{\omega(t)}{\omega_i} \\ &\times\left\{1 - \tan[\varphi(t_i)]\sin[2\int_{t_i}^{t}\omega(t_1)dt_1] + \mathcal{O}[\varphi(t)^2]\right\}.\end{aligned} \tag{15}$$

Note that there can be residual oscillations around the value obtained for a smooth turn on if $(\omega(t_i)' \neq 0)$. However, the state is still transferred adiabatically, as the uncertainty product remains constant. It is also interesting to note that the extremal values

$$\begin{aligned}\Delta\hat{z}(t_f) &= \Delta\hat{z}(t_i)\left(\frac{\omega_i}{\omega_f}\right)^{\frac{1}{2}} + \mathcal{O}[\varphi(t)] \\ &= \Delta\hat{z}(t_i)\left(\frac{U_0(t_i)}{U_0(t_f)}\right)^{\frac{1}{4}} + \mathcal{O}[\varphi(t)],\end{aligned} \tag{16}$$

$$\begin{aligned}\Delta\hat{p}(t_f) &= \Delta\hat{p}(t_i)\left(\frac{\omega_f}{\omega_i}\right)^{\frac{1}{2}} + \mathcal{O}[\varphi(t)] \\ &= \Delta\hat{p}(t_i)\left(\frac{U_0(t_f)}{U_0(t_i)}\right)^{\frac{1}{4}} + \mathcal{O}[\varphi(t)],\end{aligned} \tag{17}$$

that are reached at the end of the period are independent of the interaction time and thus also of the velocity of the

particle. This implies that within the adiabatic regime, a longitudinal velocity spread of the atomic beam has no effect on the position narrowing. However, the maximal compression is just the square root of the result that is obtained for instantaneous squeezing, which we will discuss next.

3.1.2 Instantaneous squeezing. The sudden approximation covers the other extreme case when the frequency change occurs on a time scale much shorter than an oscillation period; in other words, the state of the system is unaltered during this instant. Assuming that $\omega(t \leq t_j) = \omega_i$ remains constant until it changes instantaneously at a jump time t_j to $\omega(t > t_j) = \omega_f$, we obtain a transfer matrix $\underline{S}_{\text{sudden}}(t)$ which is formed by two harmonic-oscillator propagators (see Appendix). The position uncertainty does not change $\Delta\hat{z}(t \leq t_j) = \Delta\hat{z}(t_i)$ until the frequency jump occurs. From then on it oscillates between the initial $\Delta\hat{z}(t_i)$ and a minimal value $\Delta\hat{z}_{\min} = \Delta\hat{z}(t_i)(\omega_i/\omega_f) = \Delta\hat{z}(t_i)[U_0(t_i)/U_0(t_f)]^{1/2}$:

$$\Delta^2\hat{z}(t_i) \geq \Delta^2\hat{z}(t > t_j) = \Delta^2\hat{z}(t_i) \times \left\{1 + \left(\frac{\omega_i^2}{\omega_f^2} - 1\right)\sin[\omega_f(t - t_j)]^2\right\} \geq \Delta^2\hat{z}(t_i)\frac{\omega_i^2}{\omega_f^2}. \quad (18)$$

The momentum uncertainty also remains constant, $\Delta\hat{p}(t \leq t_j) = \Delta\hat{p}(t_i)$, before the frequency jump happens. After that time it varies periodically like

$$\Delta^2\hat{p}(t_i) \leq \Delta^2\hat{p}(t > t_j) = \Delta^2\hat{p}(t_i) \times \left\{1 + \left(\frac{\omega_f^2}{\omega_i^2} - 1\right)\sin[\omega_f(t - t_j)]^2\right\} \leq \Delta^2\hat{p}(t_i)\frac{\omega_f^2}{\omega_i^2} \quad (19)$$

between $\Delta\hat{p}(t_i)$ and a maximum of $\Delta\hat{p}_{\max} = \Delta\hat{p}(t_i)(\omega_f/\omega_i) = \Delta\hat{p}(t_i)[U_0(t_f)/U_0(t_i)]^{1/2}$. Thus, the maximal compression of the position width can be substantially larger compared to the adiabatic limit as long as the time-of-flight dispersion remains smaller than the oscillation period $2\pi/\omega_f$.

3.1.3 Non-adiabatic compression. The two aforementioned approximations are in a sense very general because they do not take into account the very details of the frequency change. By assuming the most common transverse beam profile $I(z)$, i.e., a Gaussian, we can also study the effects of a non-adiabatic turn-on. A particle passing through the profile with velocity v will experience a time-dependent oscillation frequency that is also of this shape

$$\omega(t) = \omega(0)\,e^{-\alpha(t/\tau_v)^2}, \text{ for } t_i = -\tau_v \leq t \leq t_f = 0, \quad (20)$$

where we have introduced the time-of-flight $\tau_v = L/v$ through the rising part of the profile of width $2L$. The increase in oscillation frequency from $\omega(t_i = -\tau_v) = \omega_i$ to $\omega(t_f = 0) = \omega_f$ is measured by $\alpha = \ln(\omega_f/\omega_i)$. Since there are no known solutions to (9) and (20) in terms of elementary functions, one has to resort to numerical methods to obtain the transfer matrix.

A recent publication [5] discusses an approximation, originally due to Glaser, which is especially suited for a Gaussian. Strictly speaking, the *Glaser limit* is valid only for small relative frequency changes, i.e., $\alpha = \ln(\omega_f/\omega_i) \approx (\omega_f - \omega_i)/\omega_i \ll 1$. Within this range, it is valid for all particle velocities

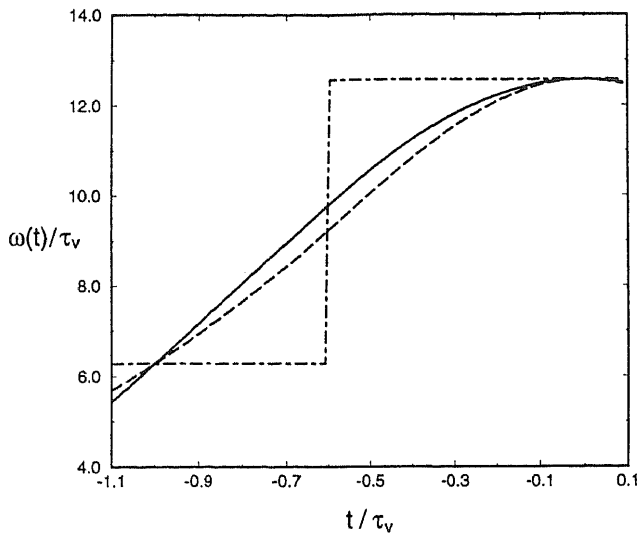

Fig. 5. Turn-on shapes $\omega(t)\tau_v$ for the three considered time-dependent frequencies vs time scaled by the time-of-flight $\tau_v = 1\,[L/v]$: Gaussian frequency $\omega_{\text{Gauss}}(t)$ (*solid*), Lorentzian frequency $\omega_{\text{Glaser}}(t)$ (*long dashed*) and the sudden frequency change $\omega_{\text{sudden}}(t)$ (*dot dashed*) where $\omega_i\tau_v = 2\pi$ and $\omega_f\tau_v = 4\pi$

$$\omega(t) = \omega_f e^{-\alpha(t/\tau_v)^2} \approx \omega_f \frac{1}{1 + \alpha\left(t/\tau_v\right)^2}. \quad (21)$$

But, even beyond these limits (i.e., $\alpha \geq 1$), the approximate Lorentzian function itself represents an interesting turn-on shape; furthermore, it interpolates between the endpoints of the Gaussian if α is set to $\alpha = (\omega_f - \omega_i)\omega_i$. The great value of this approximation lies in the fact that simple solutions are available. In this case, the position width is given by

$$\Delta^2\hat{z}[s(t)] = \Delta^2\hat{z}(t_i)\frac{1 + s^2}{1 + s_i^2}\left(1 + \left(\frac{\frac{\omega_i^2\tau_v^2}{\alpha}(1 + s_i^2)^2 + s_i^2}{q^2} - 1\right) \times \sin[\theta(s) - \theta(s_i)]^2 - \frac{s_i}{q}\sin\{2[\theta(s) - \theta(s_i)]\}\right), \quad (22)$$

where $s(t) = \sqrt{\alpha}t/\tau_v$, $\theta(s) = q\arctan s$, $q = (1 + k_v^2)^{1/2}$ and $k_v^2 = (\omega_f\tau_v)^2/\alpha$. The uninspiring expression for the momentum width can be obtained from the explicit solutions postponed to the Appendix.

In Fig. 5, we present $\omega(t)\tau_v$ for the three considered frequency turn-on shapes vs time scaled by the time-of-flight $\tau_v = 1\,[L/v]$. The solid line represents the result for the Gaussian frequency $\omega_{\text{Gauss}}(t)$, the long-dashed line is the Lorentzian approximation to it $\omega_{\text{Glaser}}(t)$, while the dot-dashed step function is $\omega_{\text{sudden}}(t)$. The frequency changes moderately from $\omega_i = 2\pi\tau_v \rightarrow \omega_f = 4\pi\tau_v$, which corresponds to a relative frequency change of $\alpha = \ln 2 = 0.69...$ Considering the non-vanishing slopes of $\omega_{\text{Gauss}}(t_i)'$ and $\omega_{\text{Glaser}}(t_i)'$, one can expect small oscillations of the position widths with a modulation frequency of $2\omega(t)$ around the value that would be obtained for a smooth turn-on as indicated in (14).

Indeed, this behavior is found in Fig. 6 where we show the position widths vs time-of-flight through the profile. We are still within the adiabatic regime as $\int_{-\tau_v}^{0}\omega(t_1)dt_1 \approx 3\pi$.

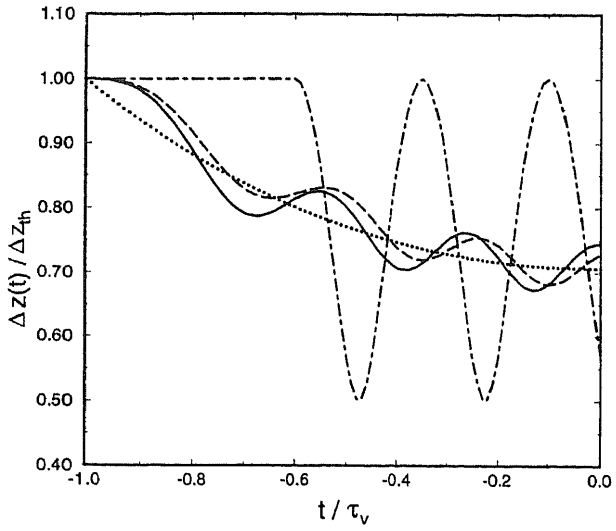

Fig. 6. Scaled position width $\Delta\hat{z}(t)/\Delta\hat{z}(t_i)$ vs time scaled by the time-of-flight $\tau_v = 1\,[L/v]$: $\Delta\hat{z}_{\mathrm{Gauss}}(t)$ (*solid line*), $\Delta\hat{z}_{\mathrm{Glaser}}(t)$ (*long dashed*), $\Delta\hat{z}_{\mathrm{sudden}}(t)$ (*dot dashed*) and for smooth adiabatic turn on $\Delta\hat{z}_{\mathrm{adiab}}(t)$ (*dotted*) where $t_j = -0.6\,\tau_v$

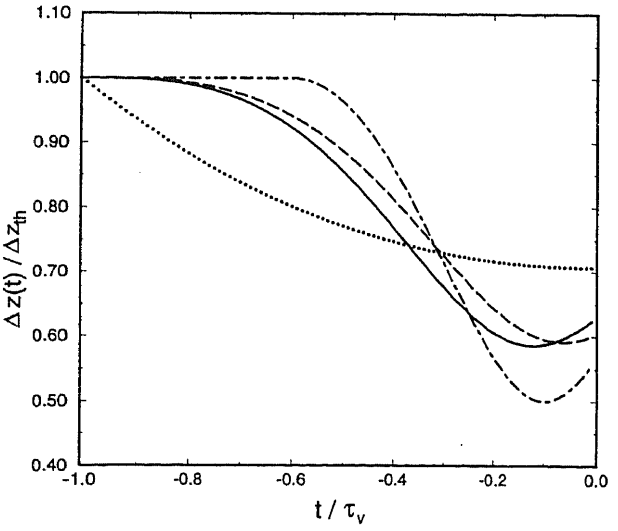

Fig. 7. Scaled position width $\Delta\hat{z}(t)/\Delta\hat{z}(t_i)$ vs time scaled by the time-of-flight $\tau_v = 0.25\,[L/v]$: $\Delta\hat{z}_{\mathrm{Gauss}}(t)$ (*solid line*), $\Delta\hat{z}_{\mathrm{Glaser}}(t)$ (*long dashed*), $\Delta\hat{z}_{\mathrm{sudden}}(t)$ (*short dashed*) and for smooth adiabatic turn on $\Delta\hat{z}_{\mathrm{adiab}}(t)$ (*dotted*), where $t_j = -0.6\,\tau_v$

The dotted curve is the adiabatic result ignoring the turn-on effect. The maximal squeezing, which is reached at $t_f = 0$ is $\Delta\hat{z}(t_f)/\Delta\hat{z}(t_i) = (\omega_i/\omega_f)^{1/2} = [U_0(t_i)/U_0(t_f)]^{1/4} = 1/\sqrt{2}$. By numerically integrating the Gaussian turn-on we obtain the solid line, while the long-dashed curve represents the result for a Lorentzian shape (22). After the frequency jump occurs at $t_j = -0.6\,\tau_v$, the postion width of the sudden limit (dot-dashed line) reaches the maximal amount of squeezing $\Delta\hat{z}(t_n)/\Delta\hat{z}(t_i) = \omega_i/\omega_f = [U_0(t_i)/U_0(t_f)]^{1/2} = 1/2$ at times $t_n = (2n+1)\,\pi/2$.

In Fig. 7, we have increased the particle velocity by a factor 4, but left all other parameters unchanged. The adiabatic character that prevails in Fig. 6 is lost now and the position widths for the continuous turn-on frequencies $\omega_{\mathrm{Gauss}}(t)$ and $\omega_{\mathrm{Glaser}}(t)$ approach the result of the sudden limit.

3.2 Adiabatic compression of the optical molasses

We have mentioned already in the previous section the advantage of the adiabatic compression over other schemes [2], i.e., its inherent insensitivity to the longitudinal velocity. In this subsection, we will examine such an adiabatic compression performed immediately after the atoms have been cooled in a rather shallow potential (since this gives the coldest temperatures in terms of the population of the various bands [9]). By increasing the depth of the optical potential, one reduces the width of the various Bloch states. Two restrictions limit the time scale of this potential increase. The compression has to be slow enough to guarantee an adiabatic evolution of the populations. A sharp drop of the potential would lead to a breathing motion of the density matrix, as has been discussed in the case of a harmonic oscillator. On the other hand, the compression has to be fast enough to avoid spontaneous emission. This would lead to heating (since the steady-state temperature increases with increasing U_0) and, therefore, result in an unwanted broadening of the spatial distribution. Defining $\Delta E(t) = E_{nq}[U_0(t)] - E_{\bar{n}q}[U_0(t)]$, the energy difference between two Bloch states as a function of the increase in potential depth, we can write conditions to both guarantee adiabaticity and avoid spontaneous emission

$$\frac{\Delta\dot{E}(t)}{\Delta E(t)} \ll \Delta E(t)/2\pi\hbar, \tag{23}$$

$$s\Gamma T \ll 1, \tag{24}$$

respectively. The first condition tells us (in conjunction with the dependence of the Bloch energies $E_n(q)$ on the potenial depth U_0) how fast we can switch on the compressing potential, and, therefore, gives us the compression time T. Condition (24) then gives us the required saturation s.

In Fig. 8, we compare the steady-state localization in the molasses and the localization obtained by compressing the atomic distribution starting from a shallow molasses ($U_0 = 100\,E_R$, $\theta = \pi/8$). The dashed line is the steady-state result from Fig. 3, while the circles refer to results we obtained from a transient simulation of cooling and successive compression processes. The solid line represents the perfectly adiabatic case which was calculated by using the steady-state populations of the various bands inferred from the molasses simulations for $U_0 = 100\,E_R$, $\theta = \pi/8$, and $\gamma_0 = 10\,\omega_R$. Using these populations as weights for the Bloch states for various potential depths, we can calculate Δz_{tot} of the resulting distribution.

In Fig. 9, we present the width of the localization, obtained for ideal adiabatic compression discussed above, but taking into account just a single Zeeman sublevel $|M_g = 3\rangle$ (solid line). In comparing this to the adiabatic compression of a thermal state of the same initial width in a harmonic oscillator (dotted line) one finds good agreement. The set of parameters is identical to those of Fig. 8.

We performed detailed simulations of the compression process for two reasons. First, due to the special form of the

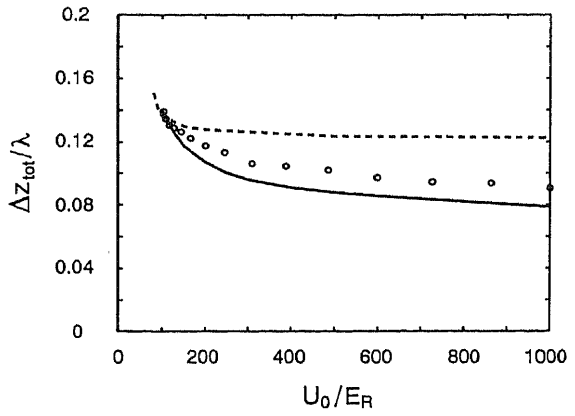

Fig. 8. Adiabatic compression, starting from a $\pi/8$ molasses with U_0=100 E_R. The *solid line* represents the perfectly adiabatic compression, calculated using the populations of the various band in the cooling molasses. The *circles* represent the results for a transient simulation with the following parameters. Cooling: $\theta=\pi/8$, U_0=100 E_R, γ_0=10 ω_R , $T_{cool} \approx 15 t_R$. Compression: $\theta=\pi/8$, U_0=100 $\longrightarrow$ 1000 E_R, γ_0=0.025 ω_R , $T_{comp} \approx 15 t_R$ [$U_0(t)$ is a Gaussian with HWHM of 8.3 t_R and a hight of 1290 E_R plus a constant background of 100 E_R]

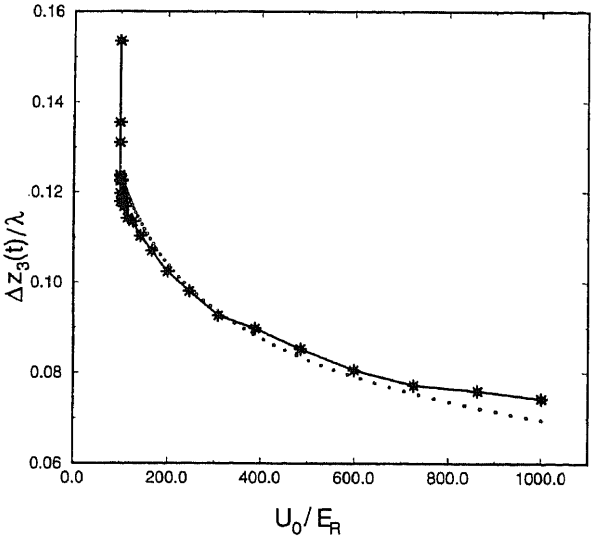

Fig. 9. Width of localization $\Delta\hat{z}_3(t)/\lambda$, for adiabatic compression if only a single Zeeman level $|M_g = 3\rangle$ is considered (*solid*) and the result of the harmonic approximation for the same initial width (*circles*). Same set of parameteres as in Fig. 8

light-shift potential (Fig. 1), the dependence of the band energies on U_0 is rather complicated and shows several avoided crossings, which correspond to the crossing of levels in the various adiabatic potentials. To maintain adiabaticity along these avoided crossings, one would have to use extremely slowly increasing potentials, which, in turn, leads to long interaction times and unrealistically small saturations. But, as the simulations show (circles in Fig. 8, see figure caption for simulation parameters), adiabaticity across these avoided crossings is not really necessary. This can be understood by the fact that only rather high-lying bands with populations of a few percent are affected by these crossings, and by the fact that diabatic transitions tend to preserve the spatial distribution of the Bloch waves.

The second reason for the simulations was to study the effect of residual spontaneous emission. The calculation shown in Fig. 8 represents the ideal case, where we decreased the saturation to such a small value that we expected (and found) only one spontaneous-emission event during the entire compression process. Using a ten times higher saturation leads to only a slight upshift of the $\Delta z_{\pm 3}$ vs U_0 characteristics that is on the same order as the Monte-Carlo uncertainty (noisiness of the data in Fig. 8).

4 Conclusions

We have investigated localization of atoms in quantized 1D optical molasses in the steady-state and transient regime in a laser configuration consisting of two linearly polarized counterpropagating laser beams with angle θ between the polarization vectors. In view to recent interest in deposition of chromium atoms on a substrate, we adopted an atomic model corresponding to an angular momentum $J_g = 3 \longrightarrow J_e = 4$ transition. Detailed results for the spatial distribution of the various Zeeman populations of the atomic ground state were presented for $\theta = \pi/2$ and $\theta = \pi/8$: in the first case, the spatial periodicity of the total atomic density is $\lambda/4$, in the second case $\lambda/2$. For the low-intensity limit investigated in this work, we found that the spatial localization was essentially constant for a potential depth larger than $\approx 100 E_R$ with FWHM on the order of $\lambda_L/10$.

Furthermore, we have investigated a time-dependent compression of the atomic distribution following the preparation of optical molasses by adiabatic compression and squeezing. For a given range of variation of the laser intensity, the best compression can be achieved by increasing the laser intensity instantaneously. The resulting breathing motion of a localized wave packet leads to a minimum width after a quarter period (squeezing). These squeezing cycles can be repeated. We emphasize, however, that the optimum compression in a squeezing scheme is the diffraction limit of coherent atom optics. A squeezing scheme requires an atomic beam with a longitudinal velocity dispersion which leads to an interaction time less than the oscillation time in the optical well. This is not the case for adiabatic compression which is independent of the interaction time or the longitudinal atomic beam velocity. For a given intensity variation, however, the compression ratio is only the square root of the squeezing scheme.

Appendix

Transfer matrices

The transfer matrix obtained in the adiabatic approximation is

$$\underline{S}_{\text{adiab}}(t,t_i) = \begin{pmatrix} \sqrt{\frac{\omega(t_i)}{\omega(t)}}\frac{\cos\left[\int_{t_i}^{t}\omega(t_1)dt_1-\varphi(t_i)\right]}{\cos\varphi(t_i)} & \frac{\sin\left[\int_{t_i}^{t}\omega(t_1)dt_1\right]}{m\sqrt{\omega(t_i)\omega(t)}} \\ -m\sqrt{\omega(t_i)\omega(t)}\frac{\sin\left[\int_{t_i}^{t}\omega(t_1)dt_1+\varphi(t)-\varphi(t_i)\right]}{\cos\varphi(t_i)\cos\varphi(t)} & \sqrt{\frac{\omega(t)}{\omega(t_i)}}\frac{\cos\left[\int_{t_i}^{t}\omega(t_1)dt_1+\varphi(t)\right]}{\cos\varphi(t)} \end{pmatrix}, \tag{A1}$$

with $\tan\varphi(t) = \omega(t)'/2\omega(t)^2$. The transfer matrix in the sudden approximation is given by

$$\underline{S}_{\text{sudden}}(t > t_j) = \underline{S}_{\omega_f}(t - t_j)\underline{S}_{\omega_i}[t_j - (-\tau_v)], \text{ with}$$

$$\underline{S}_{\omega}(t) = \begin{pmatrix} \cos\omega t & \frac{1}{m\omega}\sin\omega t \\ -m\omega\sin\omega t & \cos\omega t \end{pmatrix}. \quad \text{(A2)}$$

The transfer matrix within the Glaser limit is

$$\underline{S}_{\text{Glaser}}(t, t_i) = \underline{S}_{\text{Glaser}}[s(t)]\underline{S}_{\text{Glaser}}[s(t_i)]^{(-1)}, \quad \text{(A3)}$$

$$\underline{S}_{\text{Glaser}}[s(t) = \sqrt{\alpha}\left(\frac{t}{\tau_v}\right)]$$

$$= \begin{pmatrix} \sqrt{1+s^2}\cos\theta(s) & \frac{\tau_v\sqrt{1+s^2}}{m\sqrt{\alpha}q}\sin\theta(s) \\ m\frac{\sqrt{\alpha}}{\tau_v}\frac{s\cos\theta(s) - q\sin\theta(s)}{\sqrt{1+s^2}} & \frac{q\cos\theta(s)+s\sin\theta(s)}{q\sqrt{1+s^2}} \end{pmatrix}, \quad \text{(A4)}$$

where $\theta[s] = q\arctan s$, $q = (1 + k_v^2)^{1/2}$ and $k_v^2 = (\omega_f\tau_v)^2/\alpha$.

Acknowledgements. We thank J.J. McClelland, M. Prentiss, W. D. Phillips, and S. Rolston for discussions which initiated this work. The work at JILA is supported in part by the National Science Foundation.

References

1. G. Timp, R. E. Behringer, D. M. Tennant, J. E. Cunningham, M. Prentiss, K. K. Berggren: Phys. Rev. Lett. **69**, 1636 (1992)
2. J.J. McClelland, R.E. Scholten, E.C. Palm: Science **262**, 877 (1993)
3. V. I. Balykin, V. S. Letokhov: Opt. Commun. **64**, 151 (1987)
4. O. Carnal, M. Sigel, T. Sleator, H. Takuma, J. Mlynek: Phys. Rev. Lett. **67**, 3231 (1991)
5. J.J. McClelland, M.R. Scheinfein: J. Opt. Soc. Am. B **8**, 1974 (1991)
6. G. M. Gallatin, P. L. Gould: J. Opt. Soc. Am. B **8**, 502 (1991)
7. I. Sh. Averbukh, V. M. Akulin, W. P. Schleich: Phys. Rev. Lett. **72**, 437 (1994)
8. Y. Castin, J. Dalibard: Europhys. Lett. **14**, 761 (1991)
9. P. Marte, R. Dum, R. Taieb, P.D. Lett, P. Zoller: Phys. Rev. Lett. **71**, 1335 (1993)
10. T. Bergemann: Phys. Rev. A **48**, R3425 (1993)
11. P. S. Jessen, C. Gerz, P. D. Lett, W. D. Phillips, S. L. Rolston, R. J. C. Spreeuw, C. I. Westbrook: Phys. Rev. A **69**, 49 (1992)
12. G. Grynberg, B. Lounis, P. Verkerk, J.-Y. Courtois, C. Salomon: Phys. Rev. Lett. **70**, 2249 (1993)
13. A. Hemmerich, T. W. Hänsch: Phys. Rev. Lett. **70**, 410 (1993)
14. Adiabatic cooling of atoms in optical molasses by a slow turn-off of the optical potential has been observed experimentally at NIST Gaithersburg; W. D. Phillips, S. Rolston: Private communication (1994)
15. J. Janitzky, Y. Y. Yushin: Opt. Commun. **59**, 151 (1986)
16. G. S. Agarwal, S. A. Kumar: Phys. Rev. Lett. **26**, 3665 (1991)
17. I. Averbhuk, B. Sherman, G. Kurizki: Phys. Rev. A (submitted)
18. This squeezing limit in a finite depth optical potential with period a coincides with the diffraction limit [5] obtained for (coherent) focusing with an atomic lens of aperture a
19. P. Marte, R. Dum, R. Taieb, P. Zoller: Phys. Rev. A **47**, 1378 (1993)
20. R. Taieb, P. Marte, R. Dum, P. Zoller: Phys. Rev. A **47**, 4986 (1993)
21. Since it is well known [8] that, whenever the GOBE can be approximated by a rate equation $\gamma_0 \ll \omega_{\text{osc}} = [E_n(q) - E_{n+1}(q)]/\hbar$, the time scale for laser cooling scales with γ_0^{-1}. Within this approximation, the results of Figs. 4a,b depend only on the scaled time $\gamma_0 t$
22. P. Storey, M. Collett, D. Walls: Phys. Rev. Lett. **68**, 472 (1992)
23. M. A. M. Marte, P. Zoller: Appl. Phys. B **54**, 477 (1992)
24. B.E.A Saleh, M.C. Teich: *Fundamentals of Photonics* (Wiley–Interscience, New York 1990)